High-efficiency transition between rectangular waveguide and domino plasmonic waveguide

Article *in* AIP Advances · February 2015

DOI: 10.1063/1.4907879

7 authors, including:


Liangliang Liu
Nanyang Technological University


Zhuo Li
Nanjing University of Aeronautics & Astronautics


Bingzheng Xu
Nanjing University of Aeronautics & Astronautics

Changqing Gu
Nanjing University of Aeronautics & Astronautics

High-efficiency transition between rectangular waveguide and domino plasmonic waveguide

Cite as: AIP Advances **5**, 027105 (2015); https://doi.org/10.1063/1.4907879
Submitted: 08 November 2014 • Accepted: 29 January 2015 • Published Online: 05 February 2015

Liangliang Liu, Zhuo Li, Bingzheng Xu, et al.

AIP ADVANCES **5**, 027105 (2015)

High-efficiency transition between rectangular waveguide and domino plasmonic waveguide

Liangliang Liu, Zhuo Li,[a] Bingzheng Xu, Changqing Gu, Chen Chen, Pingping Ning, Jian Yan, and Xingyu Chen
Key Laboratory of Radar Imaging and Microwave Photonics, Ministry of Education, College of Electronic and Information Engineering, Nanjing University of Aeronautics and Astronautics, Nanjing, 210016, China

(Received 8 November 2014; accepted 29 January 2015; published online 5 February 2015)

In this work, we propose an optimized transition structure to realize smooth and high efficiency conversion from the guided wave supported by a conventional rectangular waveguide (CRW) to the domino plasmon polaritons (DPPs) supported by a domino plasmonic waveguide (DPW) and vice versa in the X-band (8.2GHz~12.4GHz). This transition structure consists of two tapered CRWs connected by a gradient domino array with optimized gradient heights and lateral widths. Experimental results of the *S*-parameters show excellent agreement with the simulations and the optimization scheme can be readily extended to other bands. Furthermore, a domino plasmonic power divider is implemented to demonstrate the application of the transition structure in the integration of conventional microwave circuits with plasmonic devices. [http://dx.doi.org/10.1063/1.4907879]

I. INTRODUCTION

Surface plasmon polaritons (SPPs) are strongly localized and confined electromagnetic (EM) mode in optical frequencies.[1–3] However, in the microwave and terahertz (THz) frequencies, the natural SPPs can not be excited for the metal behaves no longer like a plasma but resembles a perfect electric conductor (PEC). To address this issue, the idea of tailoring the topography of a PEC to allow the existence of surface modes resembling the behavior of SPPs at optical frequencies, namely spoof surface plasmon polaritons (SSPPs), was proposed and discussed in the form of two-dimensional hole lattices and one-dimensional grooves array machined into flat interfaces.[4–7] Thereafter, a number of plasmonic waveguides based on this concept have been proposed accordingly.[8–18] In these works, however, the excitations of SSPP waves are either properly polarized plane waves or monopole, which are very inefficient.

Recently, three transition structures have been successively proposed to transform the guided waves supported by a coplanar waveguide[19] or a slot line,[20] as well as a microstrip line,[21] to the SSPPs supported by an ultrathin metallic strip with symmetrical grooves, achieving high-efficiency and broadband transition performance in the microwave frequencies. Gradient grooves and a flaring ground are designed to overcome the big mismatch of the momentum and impedance between the conventional planar waveguides and the planar plasmonic waveguide.[19–21] Thus, conventional planar waveguides can efficiently excite and extract SSPP signals based on these structures. In Refs. 22 and 23, a domino array with gradient domino heights placed in a rectangular waveguide was utilized to realize a plasmonic band pass filter in the X-band. However, the transmission efficiency of this filter is not really high due to the poorly designed transition structure. Thus, high efficiency conversion from the guided waves supported by CRW to the DPPs has become necessary to realize practical three-dimensional plasmonic devices and circuits.

[a]Electronic mail: lizhuo@nuaa.edu.cn

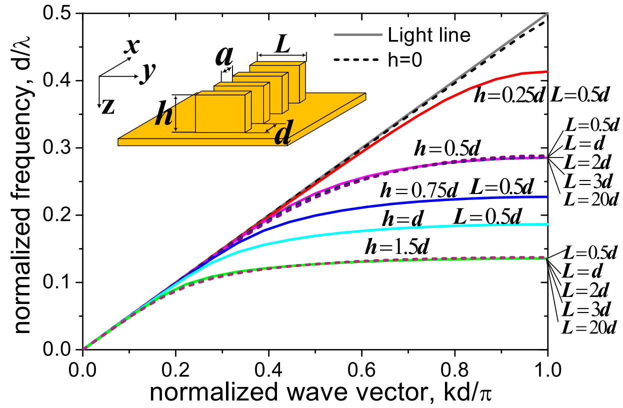

FIG. 1. Evolution of the normalized dispersion curves of a domino array on a metal surface with varying domino height h and transverse width L, in which d=5mm, a=0.6d are fixed.

In this work, we report an optimized transition structure composed of two tapered rectangular waveguides connected by a domino array with gradient heights, to achieve high efficiency and broadband conversion from the guided wave supported by a CRW to the DPPs supported by a DPW and vice versa, which is quite different from those in Refs. 22 and 23. Simulations are performed on the S-parameters and near field distributions of the proposed structure to help us optimize the specific geometrical parameters. We have also fabricated a real optimized sample and conducted experiments in the X-band. Excellent agreement between the simulation and experimental results validate our optimizations and indicate that the design scheme can be extended to other bands. Furthermore, a domino plasmonic power divider is designed to demonstrate the application of the transition structure in the integration of conventional microwave circuits with plasmonic devices.

II. DPP DISPERSIONS OF THE PLASMONIC WAVEGUIDE

To begin with, the basic properties of the DPPs are described with the dispersion characteristics, which are essential in the momentum matching for the design of the transition structure. It is a reasonable assumption that the metal can be modelled as PEC in the microwave and THz frequencies. The inset in Fig. 1 shows a DPW, which is constructed by a periodical domino array attaching to a metal plate. The array periodicity is d and domino height, lateral width and interval are denoted by h, L and a respectively. Transverse magnetic (TM) polarized waves propagating in the x direction and only the fundamental eigenmode are considered in this work. Under the conditions that $\lambda \gg a$, $\lambda \gg d$ (λ is the working wavelength), the dispersion relation can be denoted by Refs. 4 and 5 $k_x = k_0\sqrt{1 + \frac{a^2}{d^2} tan^2(k_0 h)}$, in which $k_0 = \omega/c_0$ is the wave number in free space, c_0 is the velocity of light. When $0 < k_0 h < \pi/2$, k_x will be a real number and $k_x > k_0$. Fig. 1 shows the evolution of the normalized dispersion curves of the domino array with the variation of h and L, which is obtained by the eigenmode solver of the commercial software CST Microwave Studio.[20] We notice that the asymptotic frequency is mainly controlled by the domino height h when other parameters are fixed. Within the propagation band, as h increases, the dispersion curves deviate more from the light line, which indicates the DPPs propagate more slowly and confine more tightly on the domino surface. However, when a and h are fixed, the dispersion curve is insensitive to the variation of lateral dimension L, which can be fixed to a proper value to expedite the optimizations. Thus, the domino unit's height h can be viewed the dominant parameter in the following optimizations.

III. HIGH-EFFICIENCY TRANSITION BETWEEN RECTANGULAR WAVEGUIDE AND DOMINO PLASMONIC WAVEGUIDE

Borrowing the idea of Ref. 19, the whole structure is also composed of three regions denoted in Fig. 2(a). Region I (see Fig. 2(b)) is a CRW with the cross section in the yz plane. Region

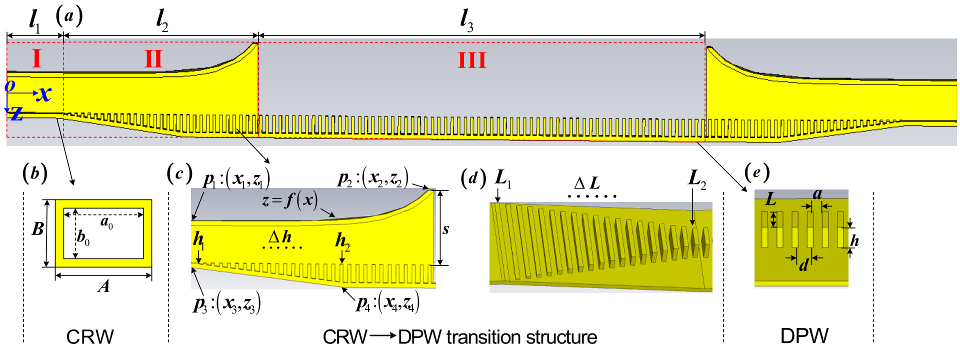

FIG. 2. (a) The schematic illustration of the whole structure with the cross-section in the xz plane. (b) The cross section of the CRW in the yz plane with the lateral dimensions of A, B, a_0 and b_0. (c) The smooth transition with gradient domino height and tapered rectangular waveguide, in which the domino height h varies from h_1 to h_2 with a step of Δh. For the tapered rectangular waveguide, the upper wall varies as a goubau line[19] and p_1 and p_2 are the start and end points of the curve z=$f(x)$, the lower wall start from p_3 to the end point p_4. (d) The domino array in the transition part with gradient lateral width L, which varies from L_1 to L_2 with a step of ΔL. (e) The DPW, in which a=0.6d, h=h_2, L=L_2.

III (see Fig. 2(e)) is a DPW with domino array in the x direction. Region II is the transition part with a gradient domino array stepping down from the lower wall of the CRW to realize smooth momentum transition and a flaring upper wall to reach impedance match between the CRW and DPW. The flaring curve in Fig. 2(c) is described as Refs. 19 and 24 $z=C_1 e^{\alpha x}+C_2$ $(x_1<x<x_2)$, where $C_1=(z_2-z_1)/(e^{\alpha x_2}-e^{\alpha x_1})$, $C_2=(z_1 e^{\alpha x_2}-z_2 e^{\alpha x_1})/(e^{\alpha x_2}-e^{\alpha x_1})$, α=0.1, $p_1(x_1,z_1)$ and $p_2(x_2,z_2)$ are the start and end points of the curve. In addition, the gradient domino height varies from h_1 to h_2 with a step of Δh, and the gradient domino lateral width varies from L_1 to L_2 with a step of ΔL. Actually, in the CRW part, we only consider the dominant mode (usually TE_{10} mode) as the excitation, whose magnetic field has only x and y components, which can effectively excite the DPPs. Through the transition part, the guided TE_{10} wave can be gradually converted to DPPs and only DPPs are supported in the DPW part.

In order to obtain an optimized transition structure, we study the variation of the S-parameters with several geometrical parameters Δh, ΔL and s (distance between P_2 and its projection to the surface of the DPW along z direction) shown in Figs. 2(c) and 2(d). First we fix L=L_1=L_2=5mm, a=1.5mm, h_2=5mm d=2.5mm and s=25mm (with goubau line). The quantitative comparison of the normalized k_x with different Δh is presented in Fig. 3(a). We notice a big momentum mismatch between the guided waves and the DPPs when Δh=5mm (h_1=0mm, h_2=5mm), in which the normalized k_x abruptly jumps from k_0 to 1.43k_0 (the red dotted line in Fig. 3(a)). When Δh gradually decreases from 5mm to 0.25mm, a smooth gradient variation of k_x value is achieved. The momentum mismatch can also be observed through S-parameters shown in Figs. 3(b) and 3(c). When Δh=5mm, the S_{11} is above -5dB from 9GHz to 11.5GHz and even above -3dB at 11GHz. In this case, more than 30% of the input powers are reflected. With the decreasing of Δh, the reflection of EM waves gradually reduces and the S_{11} is lower than -20dB from 8.2GHz to 12.4GHz when Δh=0.25mm. Similarly, as shown in Fig. 3(c), S_{21} gradually approaches 0dB when Δh becomes smaller, especially at higher frequencies.

Secondly, four different ΔL (ΔL=9mm, 4.5mm, 1mm and 0mm) are chosen to show its effect on the transmission performance shown in Figs. 4(a) and 4(b), in which Δh=0.25mm, h_2=5mm, a = 0.6d, d=5mm, L_2=5mm. We notice that the S-parameters are not sensitive to the change of ΔL, which is in accordance with the evolution of the dispersion curves varying with L in Fig. 1. So, in the following work, we set ΔL=0 (L=L_1=L_2) and study the variation of the S-parameters with different L values. In Figs. 4(c) and 4(d), we observe that if L is set as the transverse width a_0 of the rectangular waveguide, the bounded SSPP waves around the domino array will diffuse into the surrounding air and be diffracted by the side walls of the rectangular waveguide at the crossing boundary of Regions II and III, leading to bad transmission performance. When L decreases, better S_{11} will be obtained. However, S_{21} gradually deteriorates when L decreases from 14mm to 2mm, especially at lower frequencies. It

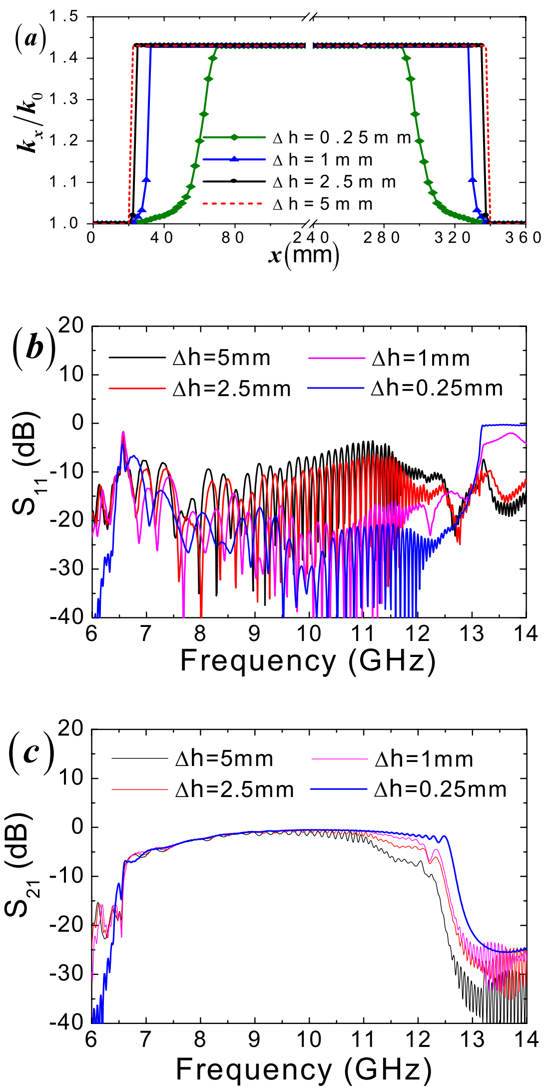

FIG. 3. (a) The variation of normalized k_x value with different Δh along the whole waveguide. (b) and (c) are the changes of S_{11} and S_{21} with different Δh, respectively.

implies that we should employ an appropriate L and it should be smaller than the lateral decay length δ_d, which is defined as the lateral distance of the DPPs away from the surface of the domino array when the magnitude of the surface electric field in the lateral space decay to γ times of the original's ($|\mathbf{E}|e^{-k_z\delta_d}=\gamma|\mathbf{E}|$,[13] $k_z=\sqrt{k_x^2-\epsilon_r k_0^2}$, ϵ_r is the relative permittivity of medium) in the whole operation frequency in the transition structure. Furthermore, the S-parameters of the proposed structure with and without goubau line are also simulated to demonstrate its effect on the transmission performance shown in Fig. 5(b), in which Δh=0.25mm, h_2=5mm, L_1=L_2=5mm, a=0.6d, d=5mm. We can observe that the transmission performance with goubau line is better than that without goubau line, especially at lower frequencies. This is due to the fact that with the goubau line s is much larger than δ_d (δ_d=16.43mm and 4.71mm when the operation frequencies are 8.2GHz and 12.4GHz respectively shown in Fig. 5(a)) in the whole X-band.

On the whole, we obtain an optimized transition structure with Δh=0.25mm, ΔL=0mm, s=25mm and L=L_1=L_2=5mm being the specific geometrical parameters.

An X-band rectangular waveguide is chosen as the feeding CRW with lateral dimensions of A=24.86mm, B=12.16mm, a_0=22.86mm, b_0=10.16mm. For the DPW part shown in Fig. 6(b), the

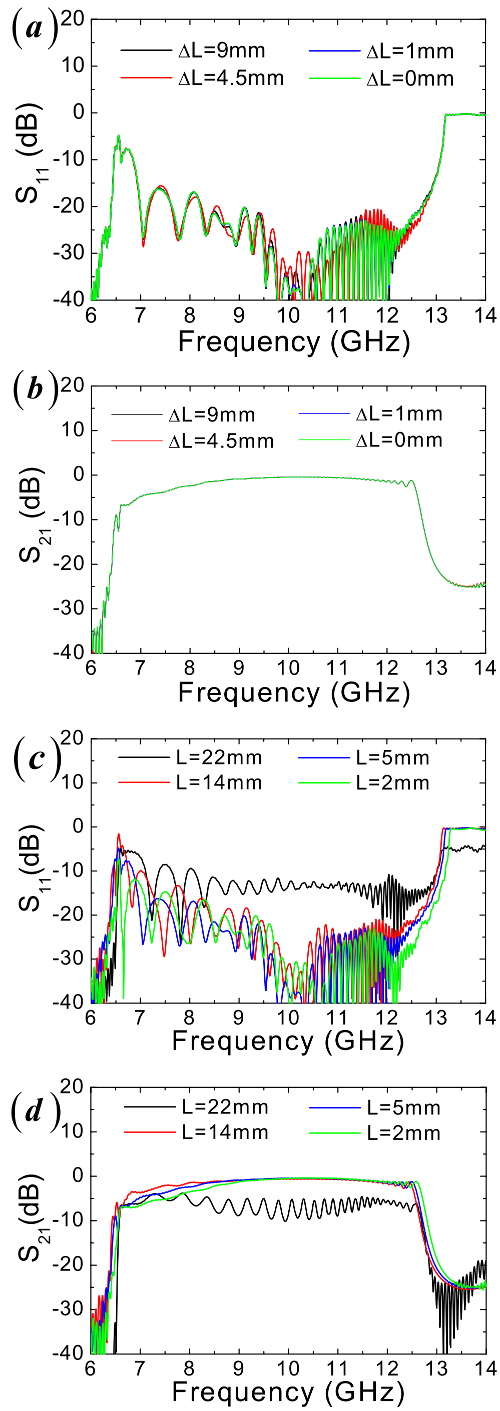

FIG. 4. (a) and (b) are the changes of S_{11} and S_{21} with different ΔL. (c) and (d) are the changes of S_{11} and S_{21} with different lateral width L in the DPW when ΔL=0.

period d=2.5mm, interval a=1.5mm, height h=5mm, lateral width L=5mm and its dispersion curve is shown in the inset in Fig. 5(a) with the cutoff frequency f_c=13.08 GHz. We remark that the dimensions of the domino array are cautiously chosen to ensure that the cutoff frequency of the DPPs is in the single mode band of the CRW. Otherwise, the transition performance could be deteriorated for the electric field intensity distribution for higher modes in the cross section can lead to

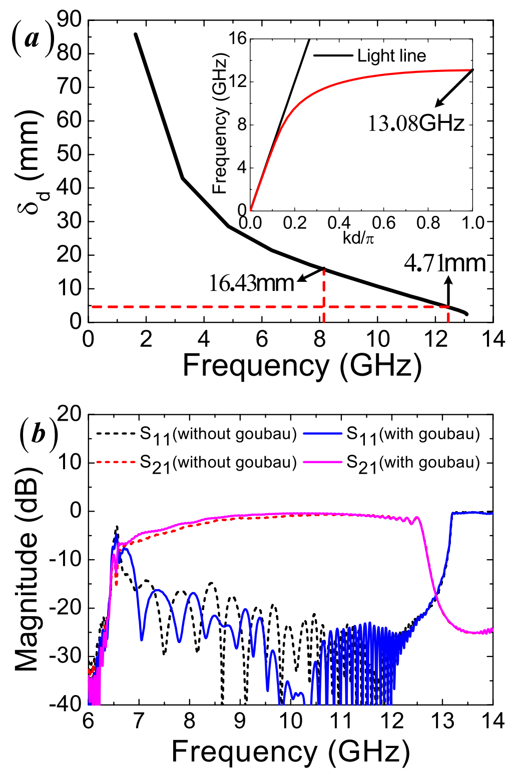

FIG. 5. (a) The lateral decay length of the DPPs propagating on the domino array filled with air (ϵ_r=1, $\gamma = 0.05$), in which d=2.5mm, a=1.5mm, L=5mm, h=5mm. The corresponding dispersion curve is shown in the inset and the cutoff frequency f_c=13.08GHz. (b) The S-parameters of the whole structure with and without goubau line in the transition part.

inefficient field confinement on the domino array setting in the middle of the rectangular waveguide. The length of each region is designed as l_1=20mm, l_2=75mm, l_3=170mm. The near-field distributions of E_z component at 10GHz on the xy plane which is 2mm away from the surface of the domino array are obtained and illustrated in Fig. 6(c). To clearly show the field conversion procedure along the waveguide, the E_z component on the yz plane at four different locations along the x coordinate

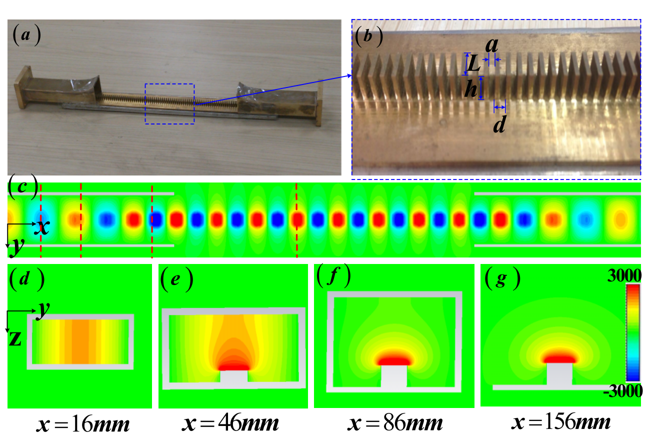

FIG. 6. (a) The fabricated sample. (b) A partial DPW. (c) The simulation near-field distributions of E_z component (V/m) at 10GHz on the xy plane which is 2mm away from the surface of the domino array. (d)-(g) The distributions of E_z on the yz plane at four different locations along x direction corresponding to the red dashed lines in (c).

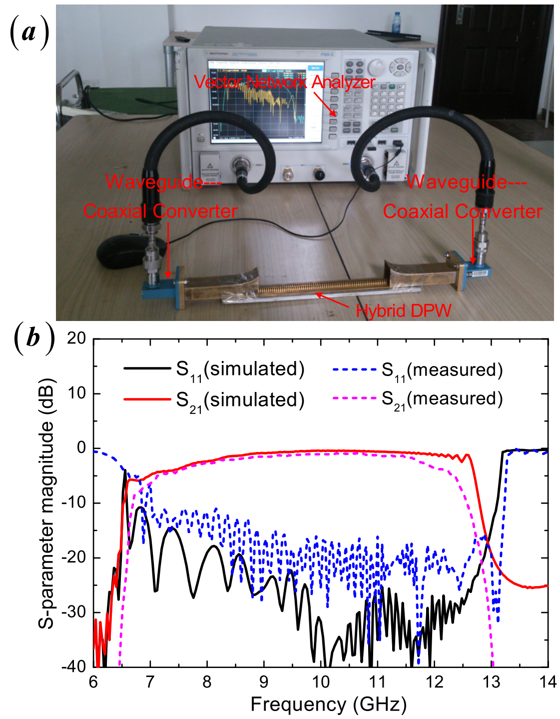

FIG. 7. (a) The setup for the S-parameters measurement. (b) The simulated and measured S-parameters of the proposed structure with the matching transition.

are shown in Figs. 6(d) to 6(g) respectively. The gradually increasing field intensity shown in Figs. 6(d) to 6(f) demonstrates how the guided waves are smoothly converted to the DPPs and tightly confined on the DPW. From Figs. 6(f) to 6(g), the field intensity remains unchanged, which imply that a complete transition is obtained and the upper and two side walls can be truncated.

To further validate the operation performance, we fabricate the whole structure by copper, which is shown in Fig. 6(a). The experimental setup consists of an Agilent N5230C vector network analyzer and two coaxial-rectangular waveguide converters for feeding and probing shown in Fig. 7(a). In order to get rid of the effect of the coaxial to rectangular waveguide transition to the overall measured S-parameters, we have made calibration to the two flanges at two ends of the structure in the measurement. The measured S-parameters are depicted in Fig. 7(b) with simulation results for comparison. It is clearly that the simulated results have good agreements with the measured ones. The reflection coefficients (S_{11}) is almost less than -10dB from 8.2GHz to 12.4GHz and the S_{21} is larger than -0.6dB from 9.5GHz to 11.5GHz. It is demonstrated that excellent conversion between the guided waves and the DPPs is achieved through the proposed transition structure.

IV. APPLICATION OF THE HIGH-EFFICIENCY TRANSITION STRUCTURE

High-efficiency and flexibility of the transition structure allow us building a variety of functional devices for microwave applications, such as power divider/combiner, directional coupler, resonator, taper *et al.*[12–16] Considering that the dispersion relation of the DPPs is rather insensitive to the waveguide width L in Fig. 1, a plasmonic power divider shown in Fig. 8(a) can be easily constructed. In which L=5mm, L^1=L^2=2.4mm, s=0.2mm and other parameters of the domino array are same as that in Fig. 6(a). The radii and angles of two bending arc lines are R_1=96mm, θ_1=27^0 R_2=99mm, θ_2=20^0 respectively (as discussed in Ref. 12, the greater the radius, the lower the loss). As shown in Fig. 8(b), the simulation near-field distributions of E_z component at 10GHz slightly above (2mm) the domino array is displayed on the xy plane. We can observe that a single

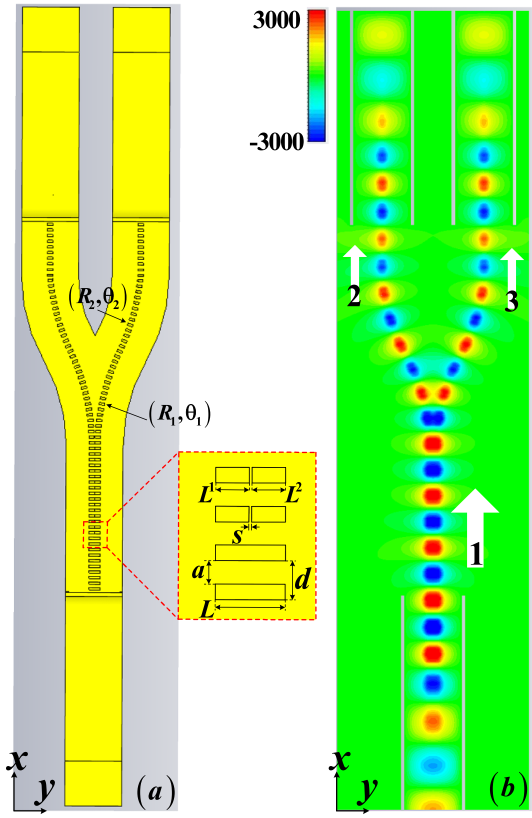

FIG. 8. The domino plasmonic power divider. (a) The cross-section of the simulation model in the *xy* plane. (b) The simulation near-field distributions of E_z component (V/m) at 10GHz is displayed on the *xy* plane slightly above (2mm) the domino array (white arrows show the direction of the poynting vectors in each chain).

DPP mode on a wide domino array (input chain 1) is split into two arms (output chains 2 and 3), and the total loss is mainly happening at the bends.[12,16] In Fig. 9, the simulation S_{11}, S_{22} and S_{33} are all below -10dB in the X-band, showing a perfect match between the DPW and CRW. S_{21} and S_{31} are the same and equal about -4dB from 9.5GHz to 12GHz, which means that the input power on chain 1 is equally divided into two output power on chains 2 and 3 respectively. In the low frequency band, the transmission loss is slightly larger due to the weak confinement of the DPPs.[12–16] In addition, a good isolation between chains 2 and 3 as S_{32} below -15dB is realized in the whole frequency bands.

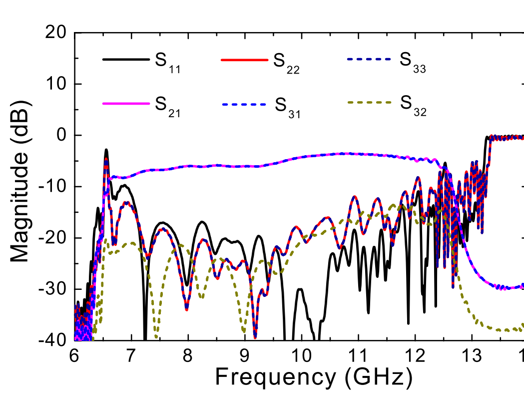

FIG. 9. The S-parameters of the domino plasmonic power divider.

V. CONCLUSION

In conclusion, we have presented an optimized transition structure to realize high efficiency and broadband conversion between the guided waves supported by the CRW and the DPPs propagating along the DPW, which consists of a tapered rectangular waveguide and a domino array with gradient heights to achieve a perfect matching between the CRW and DPW. The simulation and experimental results show excellent transmission performance in broadband. Finally, a domino plasmonic power divider is implemented to show the application of the transition structure in the integration of conventional microwave circuits with plasmonic devices.

ACKNOWLEDGMENTS

This work was supported in part by the Funding of Jiangsu Innovation Program for Graduate Education under Grant Nos. KYLX14_0275, KYLX14_0276, in part by the Fundamental Research Funds for the Central Universities under Grant No. NJ20140009, and in part by the priority academic program development of Jiangsu Higher Education Institutions.

[1] W. L. Barnes, A. Dereux, and T. W. Ebbesen, Nature **424**, 824 (2003).
[2] S. A. Maier, *Plasmonics: Fundamentals and Applications* (Springer, New York, 2007).
[3] S. I. Bozhevolnyi, V. S. Volkov, E. Devaux, J.-Y. Laluet, and T. W. Ebbesen, Nature **440**, 508 (2006).
[4] J. B. Pendry, L. Martin-Moreno, and F. J. Garcia-Vidal, Science **305**, 847 (2004).
[5] F. J. Garcia-Vidal, L. Martin-Moreno, and J. B. Pendry, J. Opt. A-Pure Appl. Opt. **7**, S97 (2005).
[6] A. P. Hibbins, B. R. Evans, and J. R. Sambles, Science **308**, 670 (2005).
[7] C. R. Williams, S. R. Andrews, S. A. Maier, A. I. Fernandez-Dominguez, L. Martin-Moreno, and F. J. Garcia-Vidal, Nat. Photon. **2**, 175 (2008).
[8] W. Zhu, A. Agrawal, and A. Nahata, Opt. Exp. **16**, 6216-6226 (2008).
[9] S. Maier, S. Andrews, L. Martin-Moreno, and F. J. Garcia-Vidal, Phys. Rev. Lett. **97**, 176805 (2006).
[10] A. I. Fernández-Domínguezf, E. Moreno, L. Martin-Moreno, and F. J. Garcia-Vidal, Phys. Rev. B **79**, 233104 (2009).
[11] A. I. Fernandez-Dominguez, E. Moreno, L. Martin-Moreno, and F. J. Garcia-Vidal, Opt. Lett. **34**, 2063-2065 (2009).
[12] D. Martin-Cano, M. L. Nesterov, A. I. Fernandez-Dominguez, F. J. Garcia-Vidal, L. Martin-Meoreno, and E. Moreno, Opt. Exp. **18**(2), 754-764 (2010).
[13] W. S. Zhao, O. M. Eldaiki, R. X. Yang, and Z. L. Lu, Opt. Exp. **18**(20), 21498-21503 (2010).
[14] M. L. Nesterov, D. Martin-Cano, A. I. Fernandez-Dominguez, E. Moreno, L. Martin-Moreno, and F. J. Garcia-Vidal, Opt. Lett. **35**(3), 423-425 (2010).
[15] Elizabeth M. G. Brock, E. Hendry, and Alastair P. Hibbins, Appl. Phys. Lett. **99**, 051108 (2011).
[16] Y. G. Ma, L. Lan, S. M. Zhong, and C. K. Ong, Opt. Exp. **19**(22), 21189-21198 (2011).
[17] D. Martin-Cano, O. Quevedo-Teruel, E. Moreno, L. Martin-Moreno, and F. J. Garcia-Vidal, Opt. Lett. **36**(23), 4635-4637 (2011).
[18] B. Gupta, S. Pandey, and A. Nahata, Opt. Exp. **22**(3), 2868-880 (2014).
[19] H. F. Ma, X. P. Shen, Q. Cheng, W. X. Jiang, and T. J. Cui, Laser Photon. Rev. **10**, 00118 (2013).
[20] X. Gao, L. Zhou, Z. Liao, H. F. Ma, and T. J. Cui, Appl. Phys. Lett. **104**, 191603 (2014).
[21] Z. Liao, J. Zhao, B. C. Pan, X. P. Shen, and T. J. Cui, J. Phys. D: Appl. Phys. **47**, 315103 (5pp) (2014).
[22] J. J. Wu, D. J. Hou, T. J. Yang, I. J. Hsieh, Y. H. Kao, and H. E. Lin, Electron. Lett. **48**(5), (2012).
[23] J. J. Wu, H. E. Lin, T. J. Yang, Y. H. Kao, H. L. Chiueh, and D. J. Hou, J. Electromagn. Analys. and Appl. **5**, 58-62 (2013).
[24] G. Goubau, IEEE Trans.Microw. Theory Techn. **4**, 197-200 (1956).